Electronic Supplementary Material (ESI) for Physical Chemistry Chemical Physics.

On the origin of preferred bicarbonate production from carbon dioxide (CO_2) capture in aqueous 2-amino-2-methyl-1-propanol (AMP)

Haley M. Stowe,[a] *Linas Vilčiauskas,*[b] *Eunsu Paek,*[b] *and Gyeong S. Hwang,*[a,b,*]

[a]Materials Science and Engineering Program and [b]McKetta Department of Chemical Engineering, University of Texas at Austin, Austin, Texas 78712, USA.

*Author to whom correspondence should be addressed:

Tel: 1-512-471-4847, Fax: 1-512-471-7060, E-mail: gshwang@che.utexas.edu

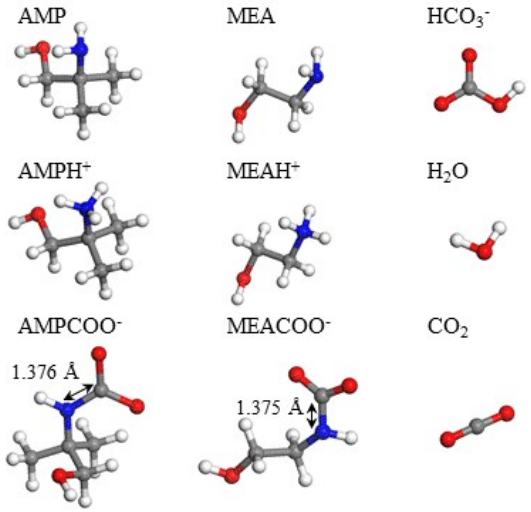

Figure S1: Structure of molecules considered in bicarbonate and carbamate formation energy predictions from AIMD simulations (Table 1) and from static QM calculations at B3LYP/6-311++G(d,p) level of theory with SMD model for implicit solvent (Table 2). The average N-C (of CO_2) bond distances (in Å) in $AMPCOO^-$ and $MEACOO^-$ from AIMD simulations are also shown. The white, grey, blue and red atoms represent H, C, N and O, respectively.

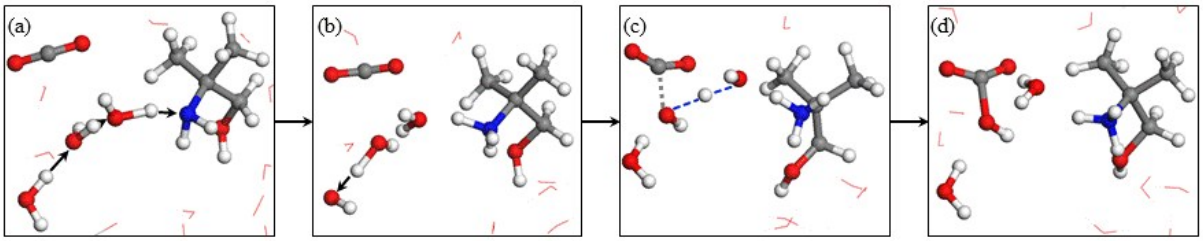

Figure S2: Snapshots from AIMD simulations of 40 wt% aqueous AMP with CO_2 at 1000 K demonstrating the occurrence of AMP + $H_2O \rightarrow AMPH^+ + OH^-$ [(a) → (b)]. This is followed by OH^- diffusion, and eventually bicarbonate formation via the $OH^- + CO_2 \rightarrow HCO_3^-$ reaction [(c) → (d)]. System contains 15 H_2O, 2 AMP, and 2 CO_2 in a 9.65 Å × 9.65 Å × 9.65 Å simulation box.

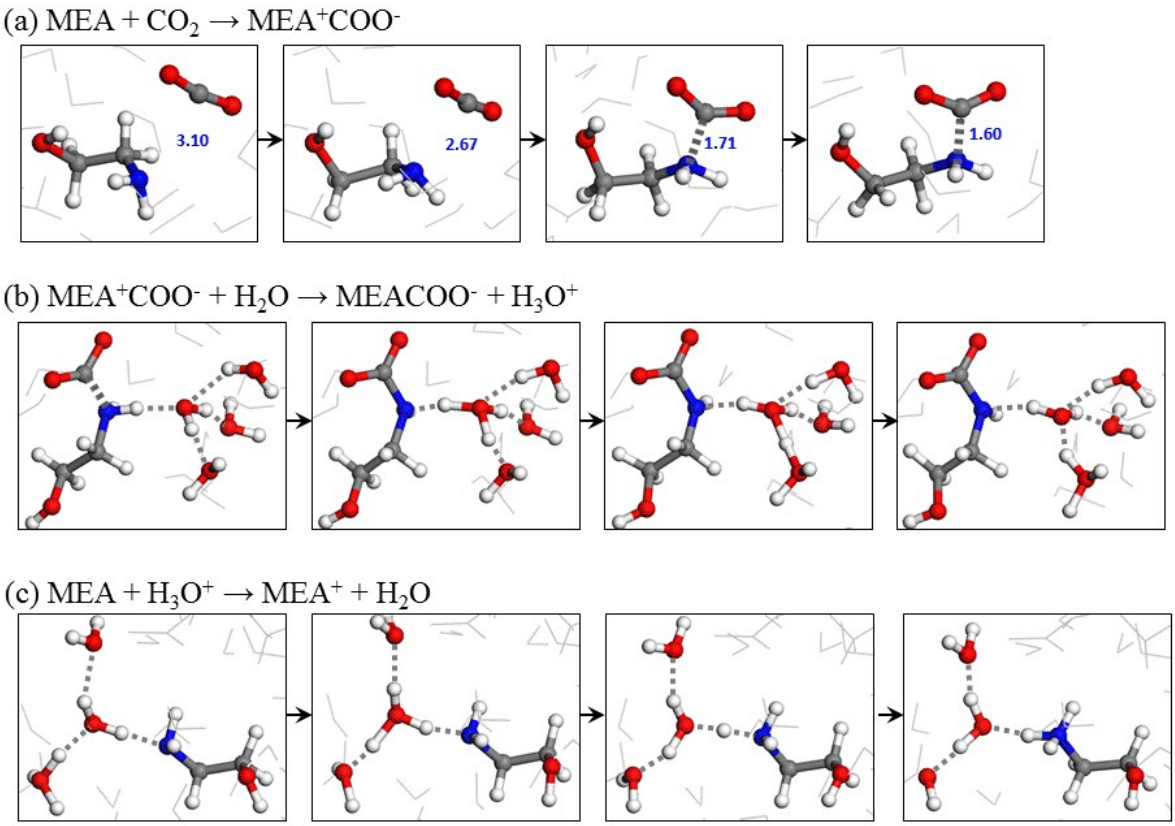

Figure S3: AIMD snapshots showing carbamate formation in 25 wt% aqueous MEA from AIMD simulations performed at 400 K. System contains 20 H_2O, 2 MEA and 1 CO_2 in a 9.278 Å × 9.278 Å × 9.278 Å simulation box. CO_2 attachment was observed within 100 ps. The system was equilibrated using classical molecular dynamics.[1]

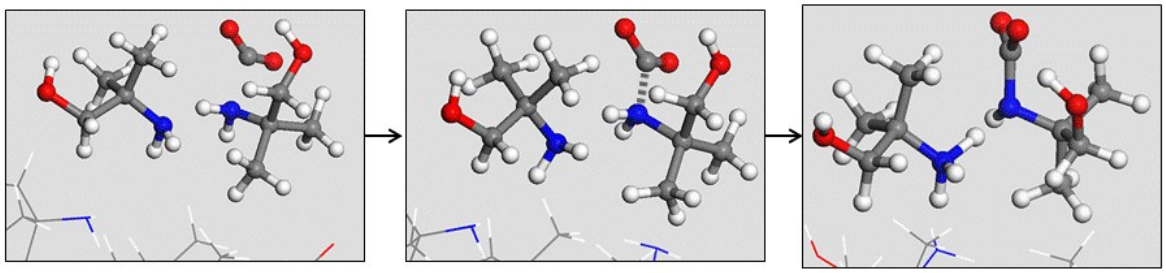

Figure S4: AIMD snapshots showing carbamate formation (AMP + CO_2 → AMP^+COO^- → $AMPH^+$ + $AMPCOO^-$) in pure AMP from AIMD simulations performed at 400 K. System contains 10 AMP and 3 CO_2 molecules in a 11.73 Å × 11.73 Å × 11.73 Å simulation box.

Table S1: Compositions and box lengths for simulation systems used in AIMD energy calculations for carbamate (2**X** + CO_2 → $\mathbf{X}H^+$ + $\mathbf{X}COO^-$) and bicarbonate (**X** + H_2O + CO_2 → $\mathbf{X}H^+$ + HCO_3^-) formation reactions shown in Table 1.

System	AMP		MEA	
	Composition	Box Length (Å)	Composition	Box Length (Å)
Initial	30 H_2O, 2 AMP, 1 CO_2	10.830	16 H_2O, 2 MEA, 1 CO_2	8.774
Carbamate	30 H_2O, 1 $AMPH^+$, 1 $AMPCOO^-$		16 H_2O, 1 $MEAH^+$, 1 MEACOO-	
Bicarbonate	29 H_2O, 1 AMP, 1 $AMPH^+$, 1 HCO_3^-		15 H_2O, 1 MEA, 1 $MEAH^+$, 1 HCO_3^-	

Reaction Energetic Calculation Details Using Implicit Solvent Model

The changes in enthalpy and Gibbs free energy in the aqueous phase (ΔH°_{aq}, ΔG°_{aq}) in Table 1 were calculated using the standard thermodynamic cycle shown below where the gaseous energy changes $(\Delta G^{\circ}_{gas}(react \rightarrow prod))$ were corrected for a difference in solvation energies ($\Delta\Delta G^{\circ}_{solv}(react \rightarrow prod)$).

$$\Delta G^{\circ}_{aq} = \sum \Delta G^{\circ}_{gas}(products) - \sum \Delta G^{\circ}_{gas}(reactants) + \sum \Delta G^{\circ}_{solv}(pro$$

$$\Delta G^{\circ}_{aq} = \Delta G^{\circ}_{gas}(react \rightarrow prod) + \Delta\Delta G^{\circ}_{solv}(react \rightarrow prod)$$

All free energies were also corrected for the change in standard state going from gas phase (1 atm) to solution (1 mol/*l*) ($\Delta G^{*}_{gas} \rightarrow \Delta G^{0}_{gas}$) by adding a factor of 7.91 kJ/mol. Following the recommendations of many authors instead of attempting to calculate the $\Delta G_{solv}(H^{+})$, $\Delta G_{solv}(OH^{-})$ and $\Delta G_{solv}(H_2O)$ we use the recommended experimental values[2], which are known to give better quantitative estimates for the overall reaction energetics.

One of the serious problems pertaining to these approaches is the presence of multiple conformations of molecules and the structural changes induced between the gaseous and polarizable continuum model (PCM) geometries. Since our study does not aim for a qualitative description of corresponding reactions, but for an elucidation of qualitative energetic trends, we only consider the most stable molecular conformations. Moreover, since we are also interested in the reaction pathways involving the carbamate zwitterionic intermediates, which are only stable in the implicit solvent, all the reactant and product geometries are referenced to the PCM ones. This means that only single point gas phase energy calculations are performed on the most stable PCM geometries. Another important source of error in PCM based approaches is their inability to correctly estimate the solvation energies of such species as hydrated proton, hydroxide and water due to the highly covalent nature of their solvation shells as well as very high solvation energies which tend to significantly amplify the computational errors. Finally, one has to keep in mind that some of these reactions already studied by a number of authors are

not isodesmic and do not conserve the number of different types of chemical bonds, which also enhance the inaccuracies in the computational methodology and limiting the quantitative usefulness of such estimates. Nevertheless, the qualitative trends in the reaction energetics are extremely useful when multiple reaction pathways have to be considered and provide valuable comparative information on the tendencies between these different pathways.

The calculated gas phase energies and solvation energies for various species considered in this study, which were used to estimate ΔH°_{aq}, and ΔG°_{aq} for the carbamate and bicarbonate reactions reported in Table 1, are reported in Table S2 below.

Table S2: Enthalpies and free energies calculated at B3LYP/6-311++G(d,p) level of theory.

	H°_{gas} (kcal/mol)	G°_{gas} (kcal/mol)	H°_{solv} (kcal/mol)	G°_{aq} (kcal/mol)	ΔH°_{solv} (kcal/mol)	ΔG°_{solv} (kcal/mol)
H_2O	-47962.80	-47976.25	-47971.36	-47984.81	-8.56	-6.67
CO_2	-118368.16	-118383.38	-118365.98	-118381.22	2.18	4.06
HCO_3^-	-165987.86	-166006.80	-166060.13	-166079.11	-72.27	-70.42
H^+		-6.29				
OH^-	-47574.95	-47587.22	-47669.80	-47682.07	-94.85	-92.95
MEA	-131999.46	-132020.59	-132010.81	-132032.03	-11.35	-9.55
MEA^+COO^-	-250346.46	-250372.59	-250377.28	-250403.54	-30.82	-29.05
$MEACOO^-$	-250023.94	-250050.20	-250103.49	-250129.01	-79.55	-76.92
$MEAH^+$	-132210.02	-132231.61	-132291.61	-132312.94	-81.59	-79.44
MEACOOH	-250367.44	-250393.56	-250384.64	-250410.88	-17.20	-15.42
AMP	-181319.16	-181343.88	-181328.82	-181353.62	-9.67	-9.74
AMP^+COO^-	-299665.31	-299695.11	-299694.87	-299724.55	-29.56	-29.44
$AMPCOO^-$	-299340.63	-299370.06	-299417.19	-299445.97	-76.56	-75.91
$AMPH^+$	-181536.37	-181561.45	-181611.75	-181636.82	-75.38	-75.37
AMPCOOH	-299682.47	-299711.80	-299697.45	-299727.83	-14.98	-16.03

Force fields employed in this work

The total energy (E_{total}) is the sum of the bond (E_{bond}), angle (E_{angle}), torsion ($E_{torsion}$) and nonbonding energies ($E_{nonbond}$). The nonbonding energy for each pair includes Colulomb interaction and van der Waals interaction in the 12-6 Lennard-Jones form. Bond and angle energies were expressed in the harmonic form. Two different forms were used to express the torsion energies, depending on the dihedral type.

$$E_{total} = E_{bond} + E_{angle} + E_{torsion} + E_{nonbond}$$

$$E_{bond} = \sum_i k_{b,i}(r_i - r_{0,i})^2$$

$$E_{angle} = \sum_i k_{\theta,i}(\theta_i - \theta_{0,i})^2$$

$$E_{torsion} = \sum_i K[1 + cos(n\emptyset - d)]$$

or

$$E_{torsion} = \sum_i [C_1 + C_2 cos(\emptyset) + C_3(\cos(\emptyset))^2 + C_4(\cos(\emptyset))^3]$$

$$E_{nonbond} = \sum_i \sum_{j>i} \left\{ \frac{q_i q_j e^2}{r_{ij}} + 4\varepsilon_{ij}\left[\left(\frac{\sigma_{ij}}{r_{ij}}\right)^{12} - \left(\frac{\sigma_{ij}}{r_{ij}}\right)^{6}\right]\right\}$$

Here, $k_{b,i}$, $k_{\theta,i}$, represent the bond and angle force constants, respectively. K, C_1, C_2, C_3, and C_4 are torsion energy coefficients, n is the periodicity of the torsion, d is the phase offset, and $\emptyset$ is the dihedral angle. $r_{0,i}$ and $\theta_{0,i}$ are the bond distance and bond angle at equilibrium, respectively. For E_{bond}, q_i is the partial atomic charge, r_{ij} is the distance between atoms *i* and *j*, ε_{ij} and σ_{ij} are the Lennard-Jones parameters which refers to the depth of the potential well and the distance where the potential is zero, respectively. A flexible version of the EPM2[3] force field was used for CO2, as presented previously[4]. The partial atomic charges for AMP and MEA were obtained from QM calculations at the B3LYP/6-311+G(d,p) level of theory and using the restrained electrostatic potential (RESP) procedure.[5] The Coulomb and L-J energies were calculated between atoms separated by three or more bonds. Although most force fields scale the 1-4 L-J and Coulomb energies, in this simulation, they were unscaled as recommended by a previous study to prevent overestimation of intramolecular hydrogen bonding in the amine species.[6] The Lorentz-Berthelot combination rule was applied for unlike atom pairs where $\varepsilon_{ij} = \sqrt{\varepsilon_i \varepsilon_i}$ and $\sigma_{ij} = (\sigma_i + \sigma_j)/2$.

Table S3: Nonbonded force field parameters

Species	Atom	q_i	σ_i (Å)	ε_i (kcal/mol)	Reference (σ_i, ε_i)
MEA	H_N	0.341	1.069	0.0157	6
	N	-0.899	3.25	0.170	
	C_N	0.176	3.3996	0.1094	
	C_O	0.338	3.3996	0.1094	
	O_H	-0.616	3.0664	0.2104	
	H_O	0.359	0.0	0.0	
	H_C	-0.010	2.4714	0.0157	
AMP	H_N	0.355	1.069	0.0157	6
	N	-1.003	3.25	0.170	
	C_N	0.625	3.3996	0.1094	
	C_O	0.112	3.3996	0.1094	
	O_H	-0.653	3.0664	0.2104	
	H_O	0.395	0.0	0.0	
	H_C	0.0435	2.4714	0.0157	7
	C_{CH3}	-0.267	3.3996	0.1094	
CO_2	O	-0.3256	3.033	0.1600	3
	C	0.6512	2.757	0.0560	

Table S4: Bond parameters

Species	Bond Type	k_b (kcal/mol/ Å^2)	r_0 (Å)	Reference
MEA AMP	N - C_N	320.6	1.470	6
	C - C	303.1	1.535	
	N - H_N	394.1	1.018	
	C_O - O_H	314.1	1.426	
	O_H - H_O	369.6	0.974	
	C - H_C	335.9	1.093	
CO_2	C-O	1283.38	1.149	k_b[8], r_0[3]

Table S5: Angle parameters

Species	Angle Type	k_θ (kcal/mol/rad^2)	θ_0 (°)	Reference
MEA AMP	C_N - N - H_N	46.0	116.78	6
	H_N - N - H_N	35.0	109.5	
	N - C_N - C	66.2	110.38	
	H_C - C - C	46.4	110.07	
	C_N - C_O - O_H	67.7	109.43	
	C_O - O_H - H_O	47.1	108.16	
MEA	H_C - C_N - N	50.0	109.5	7
MEA AMP	H_C - C - H_C	35.0	109.5	
	H_C - C_O - O_H	50.0	109.5	
AMP	C - C - C	40.0	109.5	
CO_2	O-C-O	56.53	180	k_θ[9], θ_0[3]

Table S6: Dihedral parameters (multi-harmonic form)[6]

Species	Dihedral Type	C_1 (kcal/mol)	C_2 (kcal/mol)	C_3 (kcal/mol)	C_4 (kcal/mol)
MEA AMP	H_N - N - C_N - C_O	0.59	-3.75	-1.18	3.28
	O_H - C_O - C_N - N	0.08	-4.487	-0.16	4.6224
	C_N - C_O - O_H - H_O	0.0	-0.22	0.0	-0.28

Table S7: Dihedral parameters (amber form)[7]

Species	Dihedral Type	K (kcal/mol)	n	d (°)
AMP	H_C - C_O - O_H - H_O	0.167	3	0
	X - C - C- H_C/C	0.156	3	0

References:

[1] G. S. Hwang, H. M. Stowe, E. Paek and D. Manogaran, *Phys. Chem. Chem. Phys.*, 2015, **17**, 831–839.

[2] A. V Marenich, C. J. Cramer and D. G. Truhlar, *J. Phys. Chem. B*, 2009, **113**, 6378–6396.

[3] J. G. Harris and K. H. Yung, *J. Phys. Chem.*, 1995, **99**, 12021–12024.

[4] S.-N. Huang, T. A. Pascal, W. A. Goddard, P. K. Maiti and S.-T. Lin, *J. Chem. Theory Comput.*, 2011, **7**, 1893–1901.

[5] C. I. Bayly, P. Cieplak, W. D. Cornell and P. A. Kollman, *J. Phys. Chem.*, 1993, **97**, 10269–10280.

[6] E. F. da Silva, T. Kuznetsova, B. Kvamme and K. M. Merz, *J. Phys. Chem. B*, 2007, **111**, 3695–3703.

[7] W. D. Cornell, P. Cieplak, C. I. Bayly, I. R. Gould, K. M. Merz, D. M. Ferguson, D. C. Spellmeyer, T. Fox, J. W. Caldwell and P. A. Kollman, *J. Am. Chem. Soc.*, 1995, **117**, 5179–5197.

[8] C. Nieto-Draghi, T. De Bruin, J. Pérez-Pellitero, J. B. Avalos and A. D. Mackie, *J. Chem. Phys.*, 2007, **126**, 064509.

[9] K. E. Anderson, S. L. Mielke, J. I. Siepmann and D. G. Truhlar, *J. Phys. Chem. A*, 2009, **113**, 2053–2059.